Magazine of Civil Engineering

ISSN 2712-8172

journal homepage: http://engstroy.spbstu.ru/

Research article

UDC 624.04

DOI: 10.34910/MCE.130.8

Artificial intelligence models for determining the strength of centrally compressed pipe-concrete columns with square cross-section

A.S. Chepurnenko ✉, ***B.M. Yazyev***, ***V.S. Turina***, ***V.F. Akopyan***

Don State Technical University, Rostov-on-Don, Russian Federation

✉ *anton_chepurnenk@mail.ru*

Keywords: tubular steel structures, concrete, finite element method, compressive strength, artificial neural networks, forecasting

Abstract. The article is devoted to the development of machine learning models for predicting the ultimate load during central compression of concrete-filled steel tubular (CFST) columns with square cross-section. Artificial intelligence is currently widely used in data processing and analysis, including data on the load-bearing capacity of building structures. The use of machine learning models can become an alternative to the empirical formulas from current building design codes. The models built by artificial neural networks are based on four different architectures: cascade forward backpropagation network, Elman neural network, feedforward neural network and layer recurrent neural network. The models were trained on synthetic data obtained as a result of finite element analysis of CFST columns in a simplified formulation with varying input parameters. The input parameters of the models were the outer cross-sectional size, wall thickness, concrete compressive strength and steel yield strength. The difference from previous works is the large size of the dataset, which amounts to 22308 samples. This dataset size allows to cover the entire currently possible range of changes in input parameters. The trained models showed high performance in terms of mean squared error. The correlation coefficients between predicted and target values are close to one. The developed models were also tested on experimental data for 123 samples presented in 15 different works. The best agreement with experimental data was obtained using the layer recurrent neural network model.

Citation: Chepurnenko, A.S., Yazyev, B.M., Turina, V.S., Akopyan, V.F. Artificial intelligence models for determining the strength of centrally compressed pipe-concrete columns with square cross-section. Magazine of Civil Engineering. 2024. 17(6). Article no. 13008. DOI: 10.34910/MCE.130.8

1. Introduction

In modern construction, there is a tendency to increase the height of structures and floor spans. This requires the use of columns with high load-bearing capacity at small cross-sections. One solution to this problem is the use of concrete-filled steel tubular (CFST) structures [1–3]. The reason for the high efficiency of CFST structures lies in a number of positive qualities that they possess. This is the plastic nature of destruction even when using high-strength concrete [4–6], no need for formwork, an increase in the load-bearing capacity of concrete due to its lateral compression with a steel shell [7–9], etc.

Russian set of rules 266.1325800.2016 “Composite steel and concrete structures. Design rules” contains calculation methods only for columns of circular cross-section. At the same time, square cross-section CFST columns are widely used [10–12], for which there are no design recommendations in the current Russian design codes.

Most of the existing calculation methods are based on an empirical approach [13–15], the calculation dependencies used in this case will be applicable only for a specific design solution (for example, the absence of reinforcement of the concrete core) and the type of concrete. One of the reliable ways to predict the load-bearing capacity of CFST structures is finite element modeling [16–18]. However, this approach requires analysis in a three-dimensional physically nonlinear formulation, which leads to large time costs for preparing the calculation model and the calculation itself [19].

Currently, machine learning algorithms are widely used for determining the load-bearing capacity of building structures along with analytical and numerical algorithms [20].

The authors of [21] proposed an interpretable machine learning method based on the adaptive surrogate model with adaptive neuro-fuzzy inference system (ANFIS). To train the model, the results of 99 central compression tests on square CFST columns were collected from various sources. The quality of training was assessed using 11-fold cross-validation.

In [22], an artificial neural network (ANN) model was built to determine the load-bearing capacity of CFST columns with square and circular cross-section under central and eccentric compression. The data from 3091 full-scale experiments were used to train the model. Of these, 895 experiments were conducted for centrally compressed columns of square cross-section.

In [23], the training dataset included 1022 square-section samples, of which 685 samples were short columns and 337 were slender columns. The prediction results were compared with calculations according to Eurocode 4.

The authors of [24] considered the joint use of gene expression programming and ANNs for predicting the load-bearing capacity of CFST columns with circular and square cross-section. The experimental base for training included data from 993 samples. To validate the results, comparisons were made with design codes from six different countries.

The authors of the listed works claim that surrogate models based on machine learning have an advantage over the formulas from design codes. However, ANNs and other machine learning models are, in fact, multidimensional interpolation of data, and provide reliable results only in the range of parameters in which they were trained.

Since conducting full-scale experiments is a rather expensive and time-consuming process, some researchers use synthetic data obtained from finite element modeling to form a training dataset. An example of such an approach is the work [25]. Since the modeling is performed in a three-dimensional setting, which is also a rather labor-intensive process, the final volume of the training dataset remains small. As a rule, the volume of the training dataset does not exceed 1000 samples, which does not allow covering the entire possible range of changes in material characteristics and geometric parameters.

The purpose of this work is to develop the machine learning models for predicting the load-bearing capacity of centrally compressed square-section CFST columns, which could correctly predict the ultimate load over the entire possible range of changes in the characteristics of steel and concrete, as well as the geometric characteristics of profiled square-section pipes. The size of the training dataset in this article is 22308 samples, which is tens of times larger than the size of the datasets in previous works.

2. Materials and Methods

This article considers short columns, for which deflections do not lead to any significant increase in the eccentricity of the axial force. The following values were chosen as input parameters of ANNs: cross-sectional size a (mm); pipe wall thickness t (mm); pipe material yield strength R_y (MPa); ultimate compressive strength of concrete (prismatic strength) R_b (MPa). At the output, the ANN must predict one parameter, which is the value of the ultimate load N_{ult}.

Parameters, such as the modulus of elasticity of concrete, its tensile strength, Poisson's ratio, as well as the modulus of elasticity of steel, to a certain extent also influence the load-bearing capacity of CFST columns. However, they were not included among the input parameters. For the modulus of elasticity of concrete and its tensile strength, this is explained by the fact that they are in correlation with the prismatic compressive strength [26, 27]. The initial Poisson's ratio of ordinary concrete (under elastic work of material) varies from 0.16 to 0.20 [28]. When training the models, the value presented in the Russian design codes for the reinforced concrete structures was taken (ν = 0.2). As for the modulus of elasticity of steel, it also has a small spread from 196 to 222 GPa [29], and when training the models, it was taken equal to 200 GPa.

The supervised learning method was used to train the models. Training was carried out on synthetic data obtained by finite element modeling using a simplified method given in [30]. The essence of this

technique is to reduce the three-dimensional problem of determining the stress-strain state to a two-dimensional one based on the hypothesis of plane sections. Rectangular finite elements were used to model the concrete core, and one-dimensional finite elements were used to model the steel shell. The rounding of corners in steel profile pipes was not taken into account in the calculations. A quarter of the section was considered due to the symmetry of the problem. The side size of the concrete finite element was taken to be 1/20 of the size of the concrete core. The physical nonlinearity of concrete was specified by the equations of the deformation theory of concrete plasticity by G.A. Geniev as in [30]. Steel was considered an ideal elastoplastic material. The Huber–Mises–Henky criterion was used as a yield criterion for steel. The following formulas were used as correlation relationships between the prismatic strength of concrete R_b, tensile strength R_{bt} and the initial modulus of elasticity of concrete E_0 [31]:

$$R_{bt} = 0.29 \cdot \left(\frac{R_b}{0.788} \right)^{0.6}; \quad E_0 = 1000 \cdot \frac{0.05R_b + 57}{1 + \frac{29}{3.8 + R_b}}. \tag{1}$$

The dataset containing 22308 numerical experiments was generated[1]. The range of changes in parameters a and t (Table 1) corresponded to the current Interstate standard GOST 30245-2012 “Steel bent closed welded square and rectangular section for building. Specifications”. For each value of *a* from the range, the calculation was performed with 11 values of wall thickness from t_{min} to t_{max} with a uniform step. The concrete compressive strength varied from 10 to 120 MPa in increments of 10 MPa, the yield strength of steel varied from 220 to 840 MPa in increments of 62 MPa. A fragment of the training dataset is shown in Table 2.

Table 1. Values of parameter a, as well as ranges of variation of parameter t when constructing a training dataset.

a, mm	t_{min}, mm	t_{max}, mm
100	3	8
120	3	8
140	4	8
150	4	8
160	4	8
180	5	16
200	5	12
250	6	12
300	6	22
350	6	22
400	7	22
450	7	22
500	8	22

Table 2. Fragment of the training dataset.

No.	a, mm	t, mm	R_y, MPa	R_b, MPa	N_{ult}, kN
1	100	3.00	220	10	349.71
2	100	3.45	220	10	385.27
3	100	3.91	220	10	420.72
4	100	4.36	220	10	455.76
5	100	4.82	220	10	490.38
6	100	5.27	220	10	524.59
7	100	5.73	220	10	558.38
8	100	6.18	220	10	591.76
9	100	6.64	220	10	625.31

[1] The dataset is available at the following link: https://disk.yandex.ru/i/y2y0eTlaYox3Rw.

No.	a, mm	t, mm	R_y, MPa	R_b, MPa	N_{ult}, kN
10	100	7.09	220	10	657.89
11	100	7.55	220	10	690.07
12	100	8.00	220	10	722.50
13	100	3.00	282	10	422.21
14	100	3.45	282	10	468.22
15	100	3.91	282	10	514.09
16	100	4.36	282	10	559.41
17	100	4.82	282	10	604.20
18	100	5.27	282	10	648.45
19	100	5.73	282	10	692.81
20	100	6.18	282	10	736.03
21	100	6.64	282	10	778.72
22	100	7.09	282	10	821.63
23	100	3.00	220	10	349.71
...	...	...	...	...	...
22286	500	9.27	778	120	42107.78
22287	500	10.55	778	120	43721.33
22288	500	11.82	778	120	45326.32
22289	500	13.09	778	120	46878.91
22290	500	14.36	778	120	48465.31
22291	500	15.64	778	120	49996.36
22292	500	16.91	778	120	51564.20
22293	500	18.18	778	120	53073.77
22294	500	19.45	778	120	54623.09
22295	500	20.73	778	120	56111.24
22296	500	22.00	778	120	57642.06
22297	500	8.00	840	120	40922.32
22298	500	9.27	840	120	42593.22
22299	500	10.55	840	120	44248.28
22300	500	11.82	840	120	45887.56
22301	500	13.09	840	120	47511.10
22302	500	14.36	840	120	49118.97
22303	500	15.64	840	120	50759.78
22304	500	16.91	840	120	52338.05
22305	500	18.18	840	120	53900.79
22306	500	19.45	840	120	55501.41
22307	500	20.73	840	120	57089.77
22308	500	22.00	840	120	58609.37

Several options were considered for the architecture of the ANN: cascade forward backpropagation network, Elman neural network, feedforward neural network and layer recurrent neural network. For each option, the number of hidden layers was taken to be one, the number of neurons in the hidden layer was taken to be 10, and the hyperbolic tangent was used as the activation function. ANNs with one hidden layer are among the simplest ones, but as will be shown below, one hidden layer is enough for high quality prediction with a sufficient volume of training dataset. ANN models were implemented in MATLAB software (Neural Network Toolbox). The architecture of the ANNs used is shown schematically in Fig. 1.

Levenberg–Marquardt algorithm was used to train the models. During training, the dataset was randomly divided into three parts: Training, Validation and Test in proportions of 70%, 15% and 15%, respectively. The value of the mean squared error (MSE) was chosen as a metric for the quality of training:

$$MSE = \frac{1}{n}\sum_{i=1}^{n}\left(T_i - Y_i\right)^2, \quad (2)$$

where n is the volume of the training dataset; Y_i are the ultimate load values predicted by the neural network; T_i are the target values of the ultimate load.

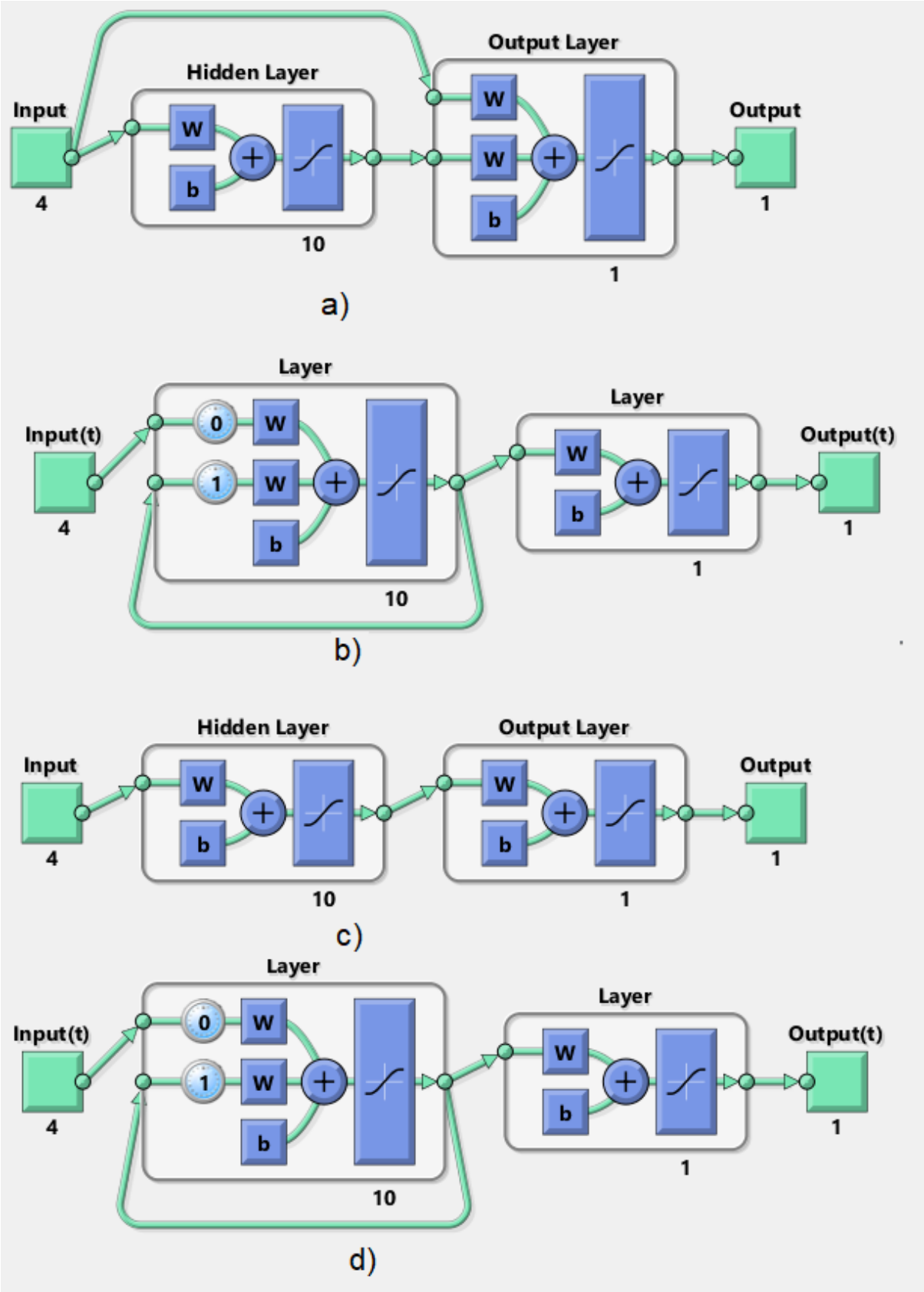

Figure 1. Architecture used for ANN: a) cascade forward backpropagation network; b) Elman neural network; c) feedforward neural network; d) layer recurrent neural network.

3. Results and Discussion

Table 3 shows the MSE values obtained as a result of models training, calculated from the "Validation" part of the dataset. The best results were obtained using the Elman architecture neural network. Training performance graph for this model is shown in Fig. 2. Fig. 3 represents regression plot for the Elman neural network model. The x axis corresponds to the target values of the ultimate loads T, and y axis corresponds to the predicted values Y. Most of the points on the graphs fit on the straight line $Y = T$. The correlation coefficients R between target and predicted values are close to 1, and for the entire sample R is equal to 0.99997. For ANN models built on cascade forward backpropagation network, feedforward neural network and layer recurrent neural network architectures correlation coefficients are also close to 1.

Table 3. MSE values obtained as a result of training ANN models.

Model	MSE
Cascade forward backpropagation network	12635.45
Elman neural network	6624.35
Feedforward neural network	9954.31
Layer recurrent neural network	7728.31

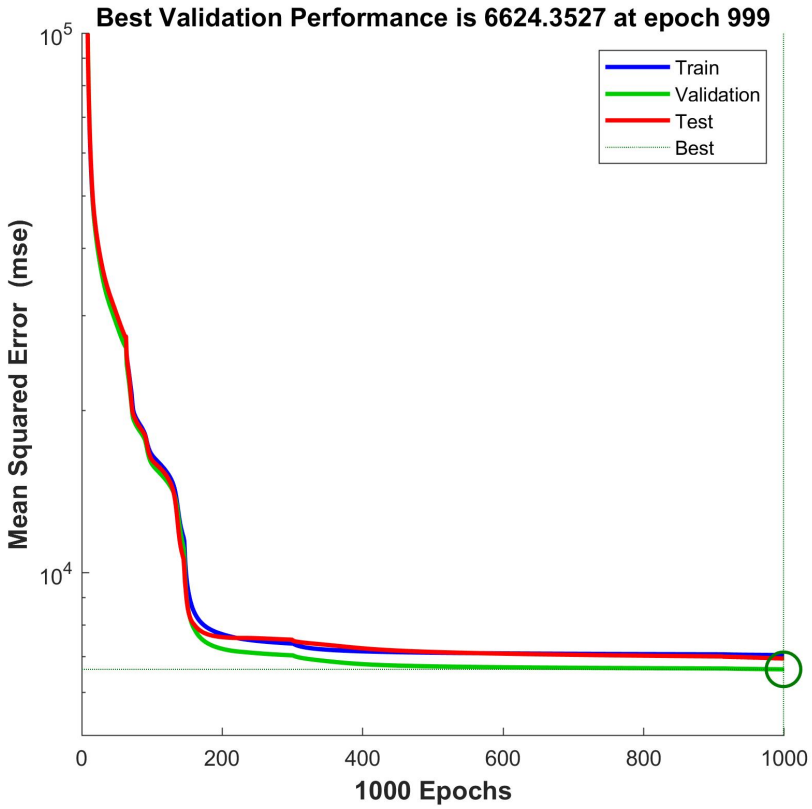

Figure 2. Training performance graph for Elman neural network.

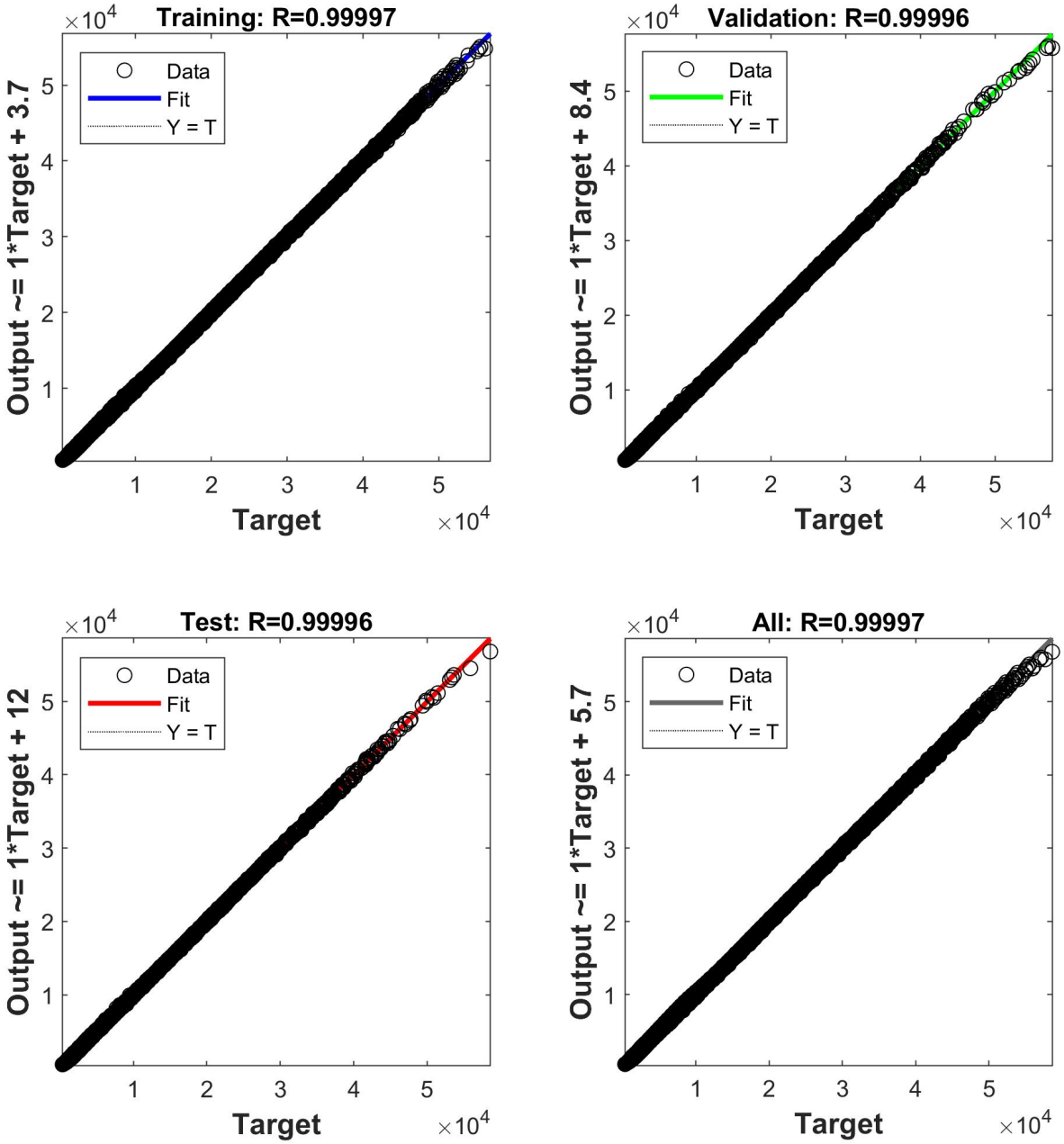

Figure 3. Regression plot for Elman neural network.

After training on synthetic data, the developed ANN models were tested on experimental data presented in [32–46]. Dimension *a* varied from 70 to 500 mm, wall thickness t varied from 0.7 to 16 mm, concrete compressive strength R_b varied from 21 to 121.6 MPa, and yield strength of steel varied from 228 to 835 MPa. The test results are given in Table 4. ANN 1 are the results obtained using cascade forward backpropagation network, ANN 2 corresponds to Elman neural network, ANN 3 corresponds to feedforward neural network and ANN 4 corresponds to layer recurrent neural network. Table 4 shows that despite the different architecture, the results predicted by the four models are quite close to each other. Table 5 shows the average values of the ratio of predicted ultimate loads $N_{predict}$ to experimental ones N_{exp}, the maximum and minimum values of the ratio $N_{predict}/N_{exp}$, standard deviations of the value $N_{predict}/N_{exp}$, as well as the coefficients of variation for each of the ANN 1–ANN 4 models.

Table 4. Results of testing the developed models on experimental data.

No.	Sample	a, mm	t, mm	R_y, MPa	R_b, MPa	N_{ult}, kN				
						experiment	ANN1	ANN2	ANN3	ANN4
Ouyang, Y., Kwan, A.K.H. (2018) [32]										
1	CR4-A-2	148	4.38	262	25.4	1153	1213	1166	1187	1178
2	CR4-A-4-1	148	4.38	262	40.5	1414	1501	1407	1453	1450
3	CR4-A-4-2	148	4.38	262	40.5	1402	1501	1407	1453	1450
4	CR4-A-8	148	4.38	262	77	2108	2135	2059	2071	2064
5	CR4-C-2	215	4.38	262	25.4	1777	2092	2052	2071	2005
6	CR4-C-4-1	215	4.38	262	41.1	2424	2746	2607	2701	2643
7	CR4-C-4-2	215	4.38	262	41.1	2393	2746	2607	2701	2643
8	CR4-C-8	215	4.38	262	80.3	3837	4304	4170	4238	4235
9	CR4-D-2	323	4.38	262	25.4	3367	3867	3947	3789	3713
10	CR4-D-4-1	323	4.38	262	41.1	4950	5358	5238	5305	5260
11	CR4-D-4-2	323	4.38	262	41.1	4830	5358	5238	5305	5260
12	CR4-D-8	324	4.38	262	80.3	7481	9212	8994	9225	9329
13	CR6-A-2	144	6.36	618	25.4	2572	2573	2563	2560	2591
14	CR6-A-4-1	144	6.36	618	40.5	2808	2850	2862	2864	2876
15	CR6-A-4-2	144	6.36	618	40.5	2765	2850	2862	2864	2876
16	CR6-A-8	144	6.36	618	77	3399	3485	3520	3502	3476
17	CR6-C-2	211	6.36	618	25.4	3920	4335	4280	4351	4346
18	CR6-C-4-1	211	6.36	618	40.5	4428	4927	4901	4980	4973
19	CR6-C-4-2	211	6.36	618	40.5	4484	4927	4901	4980	4973
20	CR6-C-8	211	6.36	618	77	5758	6335	6353	6340	6354
21	CR6-D-2	319	6.36	618	25.4	6320	7463	7402	7498	7526
22	CR6-D-4-1	319	6.36	618	41.1	7780	8879	8848	8992	9058
23	CR6-D-4-2	318	6.36	618	41.1	7473	8839	8808	8952	9017
24	CR6-D-8	319	6.36	618	85.1	10357	12996	13018	12965	13004
25	CR8-A-2	120	6.47	835	25.4	2819	2603	2592	2598	2624
26	CR8-A-4-1	120	6.47	835	40.5	2957	2815	2818	2802	2800
27	CR8-A-4-2	120	6.47	835	40.5	2961	2815	2818	2802	2800
28	CR8-A-8	119	6.47	835	77	3318	3252	3249	3189	3159
29	CR8-C-2	175	6.47	835	25.4	4210	4198	4196	4270	4272
30	CR8-C-4-1	175	6.47	835	40.5	4493	4617	4648	4680	4662
31	CR8-C-4-2	175	6.47	835	40.5	4542	4617	4648	4680	4662
32	CR8-C-8	175	6.47	835	77	5366	5581	5639	5565	5563
33	CR8-D-2	265	6.47	835	25.4	6546	7120	7089	7256	7236
34	CR8-D-4-1	264	6.47	835	41.1	7117	8052	8078	8202	8190
35	CR8-D-4-2	265	6.47	835	41.1	7172	8093	8119	8244	8232
36	CR8-D-8	265	6.47	835	80.3	8990	10537	10610	10590	10597
37	CR4-A-4-3	210	5.48	294	39.1	3183	2943	2845	2896	2860
38	CR4-A-9	211	5.48	294	91.1	4773	4909	4873	4856	4879
39	CR4-C-4-3	210	4.5	277	39.1	2713	2646	2537	2611	2562
40	CR4-C-9	211	4.5	277	91.1	4371	4641	4559	4589	4609
41	CR6-A-4-3	211	8.83	536	39.1	5898	5404	5397	5378	5360
42	CR6-A-9	211	8.83	536	91.1	7008	7280	7274	7276	7263
43	CR6-C-4-3	204	5.95	540	39.1	4026	4069	4082	4156	4136
44	CR6-C-9	204	5.95	540	91.1	5303	5932	5977	5979	5980
45	CR8-A-4-3	180	9.45	825	39.1	6803	6241	6288	6189	6165
46	CR8-A-9	180	9.45	825	91.1	7402	7506	7562	7485	7504
47	CR8-C-4-3	180	6.6	824	39.1	5028	4797	4836	4880	4849
48	CR8-C-9	180	6.6	824	91.1	5873	6235	6302	6217	6240

No.	Sample	a, mm	t, mm	R_y, MPa	R_b, MPa	N_{ult}, kN				
						experiment	ANN1	ANN2	ANN3	ANN4
Schneider, S.P. (1998) [33]										
49	S1	127.3	3.15	356	30.454	917	1080	1070	1056	1074
50	S2	126.9	4.34	357	26.044	1095	1171	1154	1136	1158
51	S3	126.95	4.55	322	23.805	1113	1101	1072	1063	1081
52	S4	125.9	5.67	312	23.805	1202	1199	1158	1160	1184
53	S5	127	7.47	347	23.805	2069	1521	1506	1494	1538
Lin, C.Y. (1988) [34]										
54	D7	150	0.7	250	23	569	743	790	748	742
55	D8	150	0.7	250	23	624	743	790	748	742
56	D10	150	1.4	250	23	726	815	844	812	804
57	D12	150	2.1	250	23	809	891	902	883	871
58	E7	150	0.7	250	34.4	762	911	912	913	903
59	E10	150	1.4	250	36	993	1023	997	1015	1003
Zhu, A. et al. (2017) [35]										
60	Pa-6-1	197	6.3	438	26.58	2730	3063	3083	3075	3062
61	Pa-6-2	198.5	6.2	438	25.81	3010	3039	3061	3052	3036
62	Pa-6-3	200.5	6.25	438	24.47	2830	3050	3072	3058	3041
63	Pa-10-1	201	10.2	382	26.58	3980	3858	3912	3849	3874
64	Pa-10-2	201	10.1	382	25.81	3920	3806	3858	3797	3821
65	Pa-10-3	199.5	10	382	24.47	3900	3694	3744	3686	3712
Yamamoto, T. et al. (2022) [36]										
66	S10D-2A	100.2	2.18	300	25.7	609	667	631	617	633
67	S20D-2A	200.3	4.35	322	29.6	2230	2232	2219	2232	2196
68	S30D-2A	300.5	6.1	395	26.5	5102	5160	5177	5151	5107
69	S10D-4A	100	2.18	300	53.7	851	884	795	804	830
70	S20D-2A	200.1	4.35	322	57.9	3201	3204	3159	3219	3208
71	S30D-4A	300.6	6.1	395	52.2	6494	7228	7185	7297	7333
72	S10D-6A	101.1	2.18	300	61	911	951	855	865	891
73	S20D-6A	200.2	4.35	322	63.7	3417	3403	3363	3417	3412
Han, L.-H. (2002) [37]										
74	rc1-1	100	2.86	228	48.3	760	836	717	745	762
75	rc1-2	100	2.86	228	48.3	800	836	717	745	762
76	rc2-1	120	2.86	228	48.3	992	1029	909	951	959
77	rc2-2	120	2.86	228	48.3	1050	1029	909	951	959
Liu, D. et al. (2003) [38]										
78	C1-1	99.25	4.18	550	70.8	1490	1544	1488	1486	1491
79	C1-2	101.05	4.18	550	70.8	1535	1578	1526	1525	1529
80	C2-1	101.05	4.18	550	82.1	1740	1682	1618	1618	1613
81	C2-2	100.55	4.18	550	82.1	1775	1671	1606	1607	1602
82	C3	182	4.18	550	70.8	3590	3747	3849	3927	3917
83	C4	181.1	4.18	550	82.1	4210	4043	4143	4195	4190
Han, L.-H., Yao, G.H. (2003) [39]										
84	M-1-1	130	2.65	340.1	22	760	909	924	889	898
85	M-1-2	130	2.65	340.1	22	770	909	924	889	898
Han, L.-H., Yao, G.H. (2004) [40]										
86	ssh-1	200	3	303.5	40	2306	2200	2177	2240	2203
87	ssh-2	200	3	303.5	40	2284	2200	2177	2240	2203
Yu, Q. et al. (2008) [41]										
88	S30-1	100	1.9	404	121.6	1209	1500	1352	1372	1377
89	S30-2	100	1.9	404	121.6	1220	1500	1352	1372	1377

No.	Sample	a, mm	t, mm	R_y, MPa	R_b, MPa	N_{ult}, kN				
						experiment	ANN1	ANN2	ANN3	ANN4
90	S30-3	100	1.9	404	121.6	1190	1500	1352	1372	1377
91	S30-4	100	1.9	404	121.6	1220	1500	1352	1372	1377
Chen, C.-C. et al. (2002) [42]										
92	AA-48	500	10	389	42.5	16500	17619	17626	17696	17633
93	AA-40	500	12	378	42.5	17900	18683	18674	18697	18672
94	AA-32	410	12	378	42.5	12800	13623	13716	13715	13765
95	AA-24	410	16	358	42.5	15300	15114	15209	15252	15279
Ding, F.-X. et al. (2014) [43]										
96	SST1-A	249.6	3.7	324.3	40.4	3131	3525	3486	3575	3529
97	SST1-B	251	3.75	324.3	40.4	2832	3575	3533	3622	3577
98	SST1-C	251.1	3.73	324.3	40.4	2677	3570	3529	3619	3573
Aslani, F. et al. (2015) [44]										
99	SC1A	70	5	701	21	1122	1085	978	964	999
100	SC2A	100	5	701	21	1417	1496	1448	1444	1477
Khan, M. et al. (2017) [45]										
101	CB15-SH (A)	74.04	4.91	762	100	1636	1708	1506	1521	1486
102	CB15-SH (B)	72.87	4.88	762	100	1755	1678	1473	1488	1453
103	CB20-SH (A)	99.56	4.91	762	100	2520	2352	2237	2234	2205
104	CB20-SH (B)	99.2	4.93	762	100	2632	2346	2229	2227	2197
105	CB25-SH (A)	124.43	4.93	762	100	3023	3159	3128	3110	3093
106	CB25-SH (B)	124.94	4.94	762	100	2962	3180	3151	3132	3116
107	CB30-SH (A)	149.99	4.92	762	100	4115	4156	4192	4162	4164
108	CB30-SH (B)	149.87	4.92	762	100	3968	4151	4187	4157	4159
Xiong, M.-X. et al. (2017) [46]										
109	S1	150	8	779	193	6536	6842	7047	6953	7581
110	S2	150	8	779	199	6715	6926	7216	7074	7793
111	S3	150	8	779	187	6616	6755	6889	6835	7380
112	S4	150	8	779	208	7276	7044	7488	7257	8135
113	S5	150	8	779	188	6974	6770	6915	6855	7413
114	S6	150	12	756	193	8585	7790	8346	8038	8807
115	S7	150	12	756	199	8452	7852	8529	8137	9009
116	S8	150	12	756	187	8687	7723	8173	7940	8618
117	S9	150	12	756	208	8730	7935	8822	8289	9335
118	S10	150	12	756	188	8912	7734	8201	7957	8648
119	S11	150	12.5	446	193	5953	5557	6194	6027	6340
120	S12	150	12.5	446	199	5911	5591	6333	6095	6444
121	S13	150	12.5	446	187	6039	5519	6061	5959	6239
122	S14	150	12.5	446	208	6409	5632	6552	6194	6609
123	S15	150	12.5	446	188	6285	5525	6083	5971	6256

Table 5. Characteristics of the quality of model forecasting.

		ANN1	ANN2	ANN3	ANN4
$N_{predict}/N_{exp}$	mean	1.046579	1.037273	1.037224	1.046729
	max	1.333582	1.388401	1.351886	1.334703
	min	0.735138	0.727888	0.722088	0.743354
Standard deviation		0.102275	0.101901	0.100931	0.097743
Coefficient of variation		9.77234	9.823902	9.730883	9.337981

Table 5 shows that quality metrics of the models are quite close, and layer recurrent neural network provides the best agreement with the experimental data. The results deviation from the experimental data can be primarily explained by the fact that when training the ANN, the simplified model of the CFST columns

deformation was used. This model did not take into account the slipping of the concrete core in the steel shell, the separation of the steel shell from the concrete core, and the effects of local buckling. In addition, of course, there was a scatter in the experimental data, which can be observed in Table 3. Our further research will be aimed at developing ANNs based on more complex theoretical models [47–48].

4. Conclusion

1. Four ANN models have been developed to predict the load-bearing capacity of centrally compressed CFST columns of square cross-section based on the following architectures: cascade forward backpropagation network, Elman neural network, feedforward neural network, layer recurrent neural network. The ANNs were trained on synthetic data obtained through a numerical experiment using a simplified method for 22308 samples.
2. The trained neural networks are characterized by low MSE, and the correlation coefficients between the predicted and target values are close to one. The best MSE value was achieved using the Elman neural network architecture that has a feedback.
3. The developed models of ANNs were tested on experimental data for 123 samples presented in 15 different papers. The model based on the layer recurrent neural network architecture, which has feedback like Elman neural network, showed the best forecasting quality. The average ratio of the predicted ultimate loads values to the experimental ones was 1.047, the maximum was 1.335, and the minimum was 0.743.
4. Further research can be aimed at training ANNs using more complex theoretical models that take into account the features of the contact interaction between the concrete core and the steel shell, the effects of local buckling, the slenderness of the elements, the presence of eccentricities, etc.

References

1. Tran, H., Thai, H.T., Ngo, T., Uy, B., Li, D., Mo, J. Nonlinear inelastic simulation of high-rise buildings with innovative composite coupling shear walls and CFST columns. The Structural Design of Tall and Special Buildings. 2021. 30(13). Article no. e1883. DOI: 10.1002/tal.1883
2. Chen, Z., Gao, F., Hu, J., Liang, H., Huang, S. Creep and shrinkage monitoring and modelling of CFST columns in a super high-rise under-construction building. Journal of Building Engineering. 2023. 76. Article no. 107282. DOI: 10.1016/j.jobe.2023.107282
3. Thai, H.-T., Thai, S., Ngo, T., Uy, B., Kang, W.-H., Hicks, S.J. Reliability considerations of modern design codes for CFST columns. Journal of Constructional Steel Research. 2021. 177. Article no. 106482. DOI: 10.1016/j.jcsr.2020.106482
4. Yuan, H.-H., She, Z.-M., Wu, Q.-X., Huang, Y.-F. Experimental and parametric investigation on elastoplastic seismic response of CFST battened built-up columns. Soil Dynamics and Earthquake Engineering. 2021. 145. Article no. 106726. DOI: 10.1016/j.soildyn.2021.106726
5. Grzeszykowski, B., Szmigiera, E.D. Experimental Investigation on the Vertical Ductility of Rectangular CFST Columns Loaded Axially. Materials. 2022. 15(6). Article no. 2231. DOI: 10.3390/ma15062231
6. Cai, W.-Z., Wang, B., Shi, Q.-X. Hysteretic model and seismic energy response of CFST columns in diagrid structure. Journal of Building Engineering. 2023. 68. Article no. 106185. DOI: 10.1016/j.jobe.2023.106185
7. Hassooni, A.N., Al Zaidee, S.R. Behavior and Strength of Composite Columns under the Impact of Uniaxial Compression Loading. Engineering, Technology & Applied Science Research. 2022. 12(4). Pp. 8843–8849. DOI: 10.48084/etasr.4753
8. Du, Y., Zhang, Y., Chen, Z., Yan, J.-B., Zheng, Z. Axial compressive performance of CFRP confined rectangular CFST columns using high-strength materials with moderate slenderness. Construction and Building Materials. 2021. 299. Article no. 123912. DOI: 10.1016/j.conbuildmat.2021.123912
9. Yang, Y., Wu, C., Liu, Z., Qin, Y., Wang, W. Comparative study on square and rectangular UHPFRC-Filled steel tubular (CFST) columns under axial compression. Structures. 2021. 34. Pp. 2054–2068. DOI: 10.1016/j.istruc.2021.08.104
10. Wu, S., Liu, W., Zhang, J., He, W., Guo, Y. Experimental and analytical investigation of square-shaped concrete-filled steel tube columns. Journal of Constructional Steel Research. 2023. 201. Article no. 107737. DOI: 10.1016/j.jcsr.2022.107737
11. Chen, J., Chan, T.-M., Chung, K.-F. Design of square and rectangular CFST cross-sectional capacities in compression. Journal of Constructional Steel Research. 2021. 176. Article no. 106419. DOI: 10.1016/j.jcsr.2020.106419
12. Zhao, P., Huang, Y., Lu, Y., Liang, H., Zhu, T. Eccentric behaviour of square CFST columns strengthened using square steel tube and high-performance concrete jackets. Engineering Structures. 2022. 253. Article no. 113772. DOI: 10.1016/j.engstruct.2021.113772
13. Yang, C., Gao, P., Wu, X., Chen, Y.F., Li, Q., Li, Z. Practical formula for predicting axial strength of circular-CFST columns considering size effect. Journal of Constructional Steel Research. 2020. 168. Article no. 105979. DOI: 10.1016/j.jcsr.2020.105979
14. Al Zand, A.W., Badaruzzaman, W.H.W., Tawfeeq, W.M. New empirical methods for predicting flexural capacity and stiffness of CFST beam. Journal of Constructional Steel Research. 2020. 164. Article no. 105778. DOI: 10.1016/j.jcsr.2019.105778
15. Jin, L., Fan, L., Li, D., Du, X. Size effect of square concrete-filled steel tubular columns subjected to lateral shear and axial compression: Modelling and formulation. Thin-Walled Structures. 2020. 157. Article no. 107158. DOI: 10.1016/j.tws.2020.107158
16. Wang, K., Chen, M., Zhang, R., Fang, W. Finite element simulation of load bearing capacity of circular CFST long columns with localized corrosion under eccentric load. Structures. 2022. 43. Pp. 1629–1642. DOI: 10.1016/j.istruc.2022.07.029
17. Sarir, P., Jiang, H., Asteris, P.G., Formisano, A., Armaghani, D.J. Iterative Finite Element Analysis of Concrete-Filled Steel Tube Columns Subjected to Axial Compression. Buildings. 2022. 12(12). Article no. 2071. DOI: 10.3390/buildings12122071

18. Liu, J., Yu, W., Fang, Y., Pan, Z., Cao, G. Finite Element Analysis on the Seismic Performance of Concrete-Filled Steel Tube Columns with a Multiple-Chamber Round-Ended Cross-Section. Buildings. 2024. 14(4). Article no. 1154. DOI: 10.3390/buildings14041154
19. Tao, Z., Katwal, U., Uy, B., Wang, W.-D. Simplified Nonlinear Simulation of Rectangular Concrete-Filled Steel Tubular Columns. Journal of Structural Engineering. 2021. 147(6). Article no. 04021061. DOI: 10.1061/(ASCE)ST.1943-541X.0003021
20. Naser, M.Z., Thai, S., Thai, H.-T. Evaluating structural response of concrete-filled steel tubular columns through machine learning. Journal of Building Engineering. 2021. 34. Article no. 101888. DOI: 10.1016/j.jobe.2020.101888
21. Le, T.-T., Phan, H.C. Prediction of Ultimate Load of Rectangular CFST Columns Using Interpretable Machine Learning Method. Advances in Civil Engineering. 2020. 1. Article no. 8855069. DOI: 10.1155/2020/8855069
22. Zarringol, M., Thai, H.-T., Thai, S., Patel, V. Application of ANN to the design of CFST columns. Structures. 2020. 28. Pp. 2203–2220. DOI: 10.1016/j.istruc.2020.10.048
23. Đorđević, F., Kostić, S.M. Practical ANN prediction models for the axial capacity of square CFST columns. Journal of Big Data. 2023. 10(1). Article no. 67. DOI: 10.1186/s40537-023-00739-y
24. Memarzadeh, A., Sabetifar, H., Nematzadeh, M. A comprehensive and reliable investigation of axial capacity of Sy-CFST columns using machine learning-based models. Engineering Structures. 2023. 284. Article no. 115956. DOI: 10.1016/j.engstruct.2023.115956
25. Tran, V.-L., Thai, D.-K., Nguyen, D.-D. Practical artificial neural network tool for predicting the axial compression capacity of circular concrete-filled steel tube columns with ultra-high-strength concrete. Thin-Walled Structures. 2020. 151. Article no. 106720. DOI: 10.1016/j.tws.2020.106720
26. Nesvetaev, G., Koryanova, Y., Kolleganov, A. E-Modulus and Creep Coefficient of Self-Compacting Concretes and Concretes with some Mineral Additives. Solid State Phenomena. 2018. 284. Pp. 963–969. DOI: 10.4028/www.scientific.net/SSP.284.963
27. Nesvetaev, G., Koryanova, Y., Chepurnenko, A. Comparison of the shear strength in heavy and self-compacting concrete. Architecture and Engineering. 2023. 8(2). Pp. 63–71. DOI: 10.23968/2500-0055-2023-8-2-63-71
28. Lu, X., Hsu, C.-T.T. Tangent Poisson's ratio of high-strength concrete in triaxial compression. Magazine of Concrete Research. 2007. 59(1). Pp. 69–77. DOI: 10.1680/macr.2007.59.1.69
29. Chen, Z., Gandhi, U., Lee, J., Wagoner, R.H. Variation and consistency of Young's modulus in steel. Journal of Materials Processing Technology. 2016. 227. Pp. 227–243. DOI: 10.1016/j.jmatprotec.2015.08.024
30. Chepurnenko, A., Yazyev, B., Meskhi, B., Beskopylny, A., Khashkhozhev, K., Chepurnenko, V. Simplified 2D Finite Element Model for Calculation of the Bearing Capacity of Eccentrically Compressed Concrete-Filled Steel Tubular Columns. Applied Sciences. 2021. 11(24). Article no. 11645. DOI: 10.3390/app112411645
31. Chepurnenko, A.S., Turina, V.S., Akopyan, V.F. Artificial intelligence model for predicting the load-bearing capacity of eccentrically compressed short concrete filled steel tubular columns. Construction Materials and Products. 2024. 7(2). Article no. 2. DOI: 10.58224/2618-7183-2024-7-2-2
32. Ouyang, Y., Kwan, A.K.H. Finite element analysis of square concrete-filled steel tube (CFST) columns under axial compressive load. Engineering Structures. 2018. 156. Pp. 443–459. DOI: 10.1016/j.engstruct.2017.11.055
33. Schneider, S.P. Axially Loaded Concrete-Filled Steel Tubes. Journal of Structural Engineering. 1998. 124(10). Pp. 1125–1138. DOI: 10.1061/(ASCE)0733-9445(1998)124:10(1125)
34. Lin, C.Y. Axial Capacity of Concrete Infilled Cold-formed Steel Columns. Proceedings of the International Specialty Conference on Cold-Formed Steel Structures. 2. University of Missouri. Rolla, 1988. Pp. 443–457.
35. Zhu, A., Zhang, X., Zhu, H., Zhu, J., Lu, Y. Experimental study of concrete filled cold-formed steel tubular stub columns. Journal of Constructional Steel Research. 2017. 134. Pp. 17–27. DOI: 10.1016/j.jcsr.2017.03.003
36. Yamamoto, T., Kawaguchi, J., Morino, S. Experimental Study of Scale Effects on the Compressive Behavior of Short Concrete-Filled Steel Tube Columns. Composite Construction in Steel and Concrete IV. 2002. Pp. 879–890. DOI: 10.1061/40616(281)76
37. Han, L.-H. Tests on stub columns of concrete-filled RHS sections. Journal of Constructional Steel Research. 2002. 58(3). Pp. 353–372. DOI: 10.1016/S0143-974X(01)00059-1
38. Liu, D., Gho, W.-M., Yuan, J. Ultimate capacity of high-strength rectangular concrete-filled steel hollow section stub columns. Journal of Constructional Steel Research. 2003. 59(12). Pp. 1499–1515. DOI: 10.1016/S0143-974X(03)00106-8
39. Han, L.-H., Yao, G.-H. Influence of concrete compaction on the strength of concrete-filled steel RHS columns. Journal of Constructional Steel Research. 2003. 59(6). Pp. 751–767. DOI: 10.1016/S0143-974X(02)00076-7
40. Han, L.-H., Yao, G.-H. Experimental behaviour of thin-walled hollow structural steel (HSS) columns filled with self-consolidating concrete (SCC). Thin-Walled Structures. 2004. 42(9). Pp. 1357–1377. DOI: 10.1016/j.tws.2004.03.016
41. Yu, Q., Tao, Z., Wu, Y.-X. Experimental behaviour of high performance concrete-filled steel tubular columns. Thin-Walled Structures. 2008. 46(4). Pp. 362–370. DOI: 10.1016/j.tws.2007.10.001
42. Chen, C.-C., Ko, J.-W., Huang, G.-L., Chang, Y.-M. Local buckling and concrete confinement of concrete-filled box columns under axial load. Journal of Constructional Steel Research. 2012. 78. Pp. 8–21. DOI: 10.1016/j.jcsr.2012.06.006
43. Ding, F.-X., Fang, C., Bai, Y., Gong, Y.-Z. Mechanical performance of stirrup-confined concrete-filled steel tubular stub columns under axial loading. Journal of Constructional Steel Research. 2014. 98. Pp. 146–157. DOI: 10.1016/j.jcsr.2014.03.005
44. Aslani, F., Uy, B., Tao, Z., Mashiri, F. Behaviour and design of composite columns incorporating compact high-strength steel plates. Journal of Constructional Steel Research. 2015. 107. Pp. 94–110. DOI: 10.1016/j.jcsr.2015.01.005
45. Khan, M., Uy, B., Tao, Z., Mashiri, F. Behaviour and design of short high-strength steel welded box and concrete-filled tube (CFT) sections. Engineering Structures. 2017. 147. Pp. 458–472. DOI: 10.1016/j.engstruct.2017.06.016
46. Xiong, M.-X., Xiong, D.-X., Liew, J.Y.R. Axial performance of short concrete filled steel tubes with high-and ultra-high-strength materials. Engineering Structures. 2017. 136. Pp. 494–510. DOI: 10.1016/j.engstruct.2017.01.037
47. Novoselov, O.G., Sabitov, L.S., Sibgatullin, K.E., Sibgatullin, E.S., Klyuev, A.V., Klyuev, S.V., Shorstova, E.S. Method for calculating the strength of massive structural elements in the general case of their stress-strain state (parametric equations of the strength surface). Construction Materials and Products. 2023. 6(2). Pp. 104–120. DOI: 10.58224/2618-7183-2023-6-2-104-120
48. Novoselov, O.G., Sabitov, L.S., Sibgatullin, K.E., Sibgatullin, E.S., Klyuev, A.S., Klyuev, S.V., Shorstova, E.S. Method for calculating the strength of massive structural elements in the general case of their stress-strain state (kinematic method). Construction Materials and Products. 2023. 6(3). Pp. 5–17. DOI: 10.58224/2618-7183-2023-6-3-5-17

Information about the authors:

Anton Chepurnenko, *Doctor of Technical Sciences*
ORCID: https://orcid.org/0000-0002-9133-8546
E-mail: anton_chepurnenk@mail.ru

Batyr Yazyev, *Doctor of Technical Sciences*
ORCID: https://orcid.org/0000-0002-5205-1446
E-mail: ps62@yandex.ru

Vasilina Turina, *PhD in Technical Sciences*
ORCID: https://orcid.org/0009-0001-6399-401X
E-mail: vasilina.93@mail.ru

Vladimir Akopyan, *PhD in Technical Sciences*
ORCID: https://orcid.org/0000-0003-3976-9346
E-mail: vovaakop@mail.ru

Received: 08.07.2024. Approved after reviewing: 31.08.2024. Accepted: 03.09.2024.